ACS APPLIED NANO MATERIALS

www.acsanm.org Article

Surface-Modified Metal Oxides for Ultrasensitive Electrochemical Detection of Organophosphates, Heavy Metals, and Nutrients

Krishna Jangid, Rakesh P. Sahu, Sadman Sakib, Igor Zhitomirsky, and Ishwar K. Puri*

Cite This: https://doi.org/10.1021/acsanm.2c04105 Read Online

ACCESS | Metrics & More | Article Recommendations | Supporting Information

ABSTRACT: One method for reliable on-site detection of water pollutants is to use highly sensitive and specific nonenzymatic electrochemical sensors containing agglomeration-free detecting agents specific to the water pollutants. We describe a facile and highly effective method to fabricate electrocatalytic electrodes with ZrO_2, MnO_2, and MgO that are well dispersed within the ink used to print these electrodes. The inorganic metal oxides serve as detecting agents with specific affinity toward fenitrothion (FT, an organophosphate), lead (Pb^{2+}, a heavy-metal ion), and nitrite (NO_2^-, a nutrient), respectively. Our bioinspired method utilizes a catechol molecule, 3,4-dihydroxybenzaldehyde (DHBA), and film-forming polymer chitosan (CHIT). Redox-active DHBA strongly adsorbs the metal oxide through bidentate bonding, and CHIT-linked DHBA assists in stable film formation. This metal oxide surface modification through the DHBA-CHIT chemistry enhances the electronic, film-forming, and nanoparticle dispersing properties of the electrode modifying ink. The ink is drop-cast on nitrogen−sulfur co-doped activated carbon-coated carbon nanotubes (NS-AC-MWCNT) on a modified glassy carbon electrode (GCE). The resulting sensor consists of metal oxide as a detecting agent and NS-AC-MWCNT as a supportive electrode. The technique enhances the total surface area of the X-DHBA-CHIT/NS-AC-MWCNT/GCE electrode (where X denotes ZrO_2, MnO_2, or MgO) and its electrocatalytic properties. The ZrO_2-DHBA-CHIT/NS-AC-MWCNT/GCE sensor has an excellent detection limit of 1.69 nM for 0.01−40 μM FT, which exceeds that of enzyme-based sensing. It is reliable for lake water with a detection limit of 11.3 nM FT, attributed to its excellent antifouling ability, and has negligible interference from commonly found chemicals in drinking water. Similarly, the MnO_2-DHBA-CHIT/NS-AC-MWCNT/GCE and MgO-DHBA-CHIT/NS-AC-MWCNT/GCE sensors show excellent Pb^{2+} and NO_2^- electrochemical detection compared to unmodified electrodes. This simple, effective, non-hazardous methodology can be extended to modify the surfaces of other metal or metal oxide detecting agents.

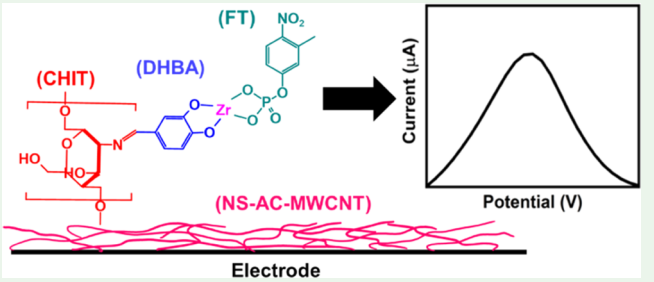

KEYWORDS: *water pollutants, metal oxides, electrochemical sensors, organophosphate, heavy-metal ion, nutrient*

1. INTRODUCTION

Population growth and urbanization have degraded water quality[1] by increasing the consumption and secretion of industrial chemicals,[2] such as organophosphorus compounds, heavy metals, and nutrients, that are major water pollutants of concern.[2−4] Organophosphorus compounds, which accrue from agricultural pesticides, impact human health and can lead to mental disorders, coma, and death.[3,5] Heavy metals like lead, cadmium, and zinc are non-biodegradable and toxic, where even tiny amounts harm multiple organs and cause neurological diseases like Alzheimer's.[2,6] While inorganic nutrients such as nitrites and nitrates are widely used in the chemical and food industries, being carcinogens, their bioaccumulation or uptake can lead to poisoning and even cancer with prolonged exposure.[7,8] Water quality issues are estimated to cost $210 billion yearly in USA alone.[4] Hence, the accurate determination of water pollutants is necessary to control their environmental footprints.

Analytical detection of water pollutants is typically conducted through mass spectrometry,[9,10] gas/liquid chromatography,[10,11] spectroscopy,[2,12] or optical colorimetry.[13] These techniques require skilled professionals, significant labor for complex sample preparation, and expensive instruments.[14] Electrochemical techniques are cost-effective and respond quickly on-site with high sensitivity.[3,15] Enzyme-based electrochemical sensors are common since they are sensitive and specific toward pollutants[16−18] but are prone to denaturation.[3,19] Nonenzymatic electrochemical sensors can overcome this limitation.

Received: September 16, 2022
Accepted: October 26, 2022

The working electrode of an electrochemical sensor, which provides the electrode−electrolyte interface required for redox reactions, benefits from faster electrode kinetics and a higher electrode surface area.[19,20] Electrode modification with nanomaterials includes use of carbon nanotubes, graphene, and metal nanoparticles.[21] An example is the synthesis of a highly conductive and porous nanomaterial containing nitrogen−sulfur codoped activated carbon-coated carbon nanotubes (NS-AC-MWCNT) for organophosphorus compound detection.[19] Since the performance of an enzymatic sensor is typically superior to that of an electrocatalytic sensor,[22,23] we hypothesize that a detecting agent to enhance the analyte concentration near the electrode−electrolyte interface would also enhance sensing performance. As per this hypothesis, incorporating analyte-capturing detecting agents is a missing key for improving the sensitivity and specificity of nonenzymatic electrochemical sensors.

Inorganic metal oxides have affinity toward several water pollutants. For instance, ZrO_2, MnO_2, and MgO have strong affinity toward concerned phosphorus compounds,[5,24] lead,[25] and nitrite,[26] respectively. Since metal oxides are readily functionalized[27] and electrocatalytic,[28] electrodes modified with these materials are employed for electrochemical detection.[28] However, metal oxides tend to agglomerate in suspension due to van der Waals forces, producing large aggregates in an ink suspension that result in poor film formation during deposition on an electrode.[29] This reduces the electrode surface area and subsequent electrocatalytic ability. While ZrO_2-based electrochemical sensors are employed for specific organophosphorus pesticide detection,[5,24] ZrO_2 suffers from agglomeration, lower electrical conductivity, and surface area. The incorporation of ZrO_2 into conductive composites has not achieved the performance of a similar enzymatic sensor.[24,30] Likewise, MnO_2-based electrochemical sensors do not approach the performance of enzymatic sensors for heavy-metal detection.[31] In addition, the utilization of MgO for affinity-based electrochemical detection of nitrite has not yet been explored. A modified electrode should also be stable during washing and voltammetry scanning for reliable and repeatable current response. Hence, electrode modification for improving sensing performance with a metal oxide is challenging.

Our goal is to overcome these challenges using an approach where the inorganic metal oxides (1) have a well-dispersed nanoparticle distribution that enhances the electrode surface area and analyte capture, (2) form a stable film on the electrode for reliable faradic current response, and (3) participate in charge transfer, thus working with conductive elements in enhancing the overall electrochemical response. We address these challenges based on a bioinspired method to produce a material with film-forming, redox-active, and strong metal oxide adhesion properties.

Catechol-containing molecules are widely used to modify metal oxide surfaces.[32,33] They adsorb metal oxides when the catechol moiety forms a strong bidentate-type bond with metal atoms.[33] The bonding mechanism is inspired by the firm adherence of a mussel to surfaces in aqueous conditions.[34] 3,4-Dihydroxybenzaldehyde (DHBA) is a catechol molecule that adsorbs and disperses TiO_2 molecules that have enhanced electronic properties[35] where the redox-active DHBA forms a charge transfer complex with the adsorbed TiO_2.[36] However, DHBA-modified TiO_2 has poor film-forming properties.[35] This catecholate molecule has terminating −COH groups, which serve as linkers. Chitosan is an organic polymer with excellent film-forming properties and can be linked to DHBA using the Schiff base reaction[33] as a result of imine bond formation between the amine and aldehyde groups of chitosan (CHIT) and DHBA, respectively. Hence, CHIT-linked DHBA chemistry can produce well-dispersed and stable inorganic metal oxide-based electrode films.[35]

We also hypothesize that with DHBA-CHIT modification, ZrO_2, MnO_2, and MgO metal oxides with an affinity toward specific water pollutants produce uniformly coated stable electrode films that enhance the overall electrochemical performances. To assess the hypothesis, we add metal oxide powder to DHBA-CHIT solution and drop-cast on an NS-AC-MWCNT-modified glassy carbon electrode (GCE). The catechol-modified metal oxides are expected to work synergistically with the NS-AC-MWCNT nanomaterial to produce electrocatalytic electrodes with an enhanced surface area and electrode kinetics.

We employ scanning electron microscopy (SEM) to investigate morphology changes and Fourier transfer infrared spectroscopy (FTIR) to characterize the chemical structure during the steps of metal oxide surface modification. Electrochemical characterizations, including electrochemical impedance spectroscopy (EIS), cyclic voltammetry (CV), and square-wave voltammetry (SWV), are used to systematically evaluate electrode electrochemical performance. SWV is also used to optimize the faradic current response for fenitrothion (FT, an organophosphate) detection. Finally, we investigate heavy-metal (Pb^{2+}) and nutrient (NO_2^-) detection with MnO_2-DHBA-CHIT/NS-AC-MWCNT and MgO-DHBA-CHIT/NS-AC-MWCNT composite electrodes. These novel composites could be integrated into a single sensor to detect organophosphates, heavy-metal ions, and nutrients in water. This simple, effective, non-hazardous metal oxide surface modification method produces a new class of specific and sensitive sensors based on metal or metal oxides.

2. MATERIALS AND METHODS

2.1. Chemicals and Instruments. Chitosan (degree of deacetylation of 85%), 3,4-dihydroxybenzaldehyde, acetate buffer solution (ABS), fenitrothion, lead iodide, sodium nitrite, acetic acid, zirconium oxide nanopowder, and magnesium oxide nanopowder were obtained from Sigma-Aldrich, Canada. Manganese dioxide was purchased from Fisher Scientific. Multiwalled carbon nanotubes were purchased from Bayer Inc., Germany. Lake water was sourced from Bayfront Park (Hamilton, Ontario). All reagents and deionized water (DI) were utilized as-received. The stock solution of FT was prepared in ethanol and refrigerated at 4 °C until use. The stock solution of Pb^{2+} was prepared in dimethylformamide, while DI water was used for the NO_2^- stock solution.

An electrochemical potentiostat (PARSTAT 2273, Princeton Applied Research) was used for cyclic voltammetry, square-wave voltammetry, and electrochemical impedance spectroscopy. A three-electrode setup, including a glassy carbon electrode (working electrode), platinum electrode (counter electrode), and Ag/AgCl electrode (reference electrode), was used to establish the electrochemical sensor. Material characterization was conducted with a JEOL 6610LV scanning electron microscope, where a silicon wafer was used for the substrate on which the synthesized material was deposited, and Fourier transform infrared spectroscopy (FTIR) was performed for powdered materials using a Bruker Vertex 70 instrument.

2.1.1. ZrO_2, MnO_2, and MgO Surface Modification. Surface modification of ZrO_2, MnO_2, and MgO was conducted using aqueous suspensions. For ZrO_2 nanoparticles, aqueous suspensions of bare

https://doi.org/10.1021/acsanm.2c04105
ACS Appl. Nano Mater. XXXX, XXX, XXX−XXX

Scheme 1. (A) Scheme of Metal Atom Surface Modification with (i) DHBA, (ii) CHIT, and (iii) DHBA-CHIT; (B) Scheme of Step-by-Step Electrode Fabrication for Electrochemical Detection of the Water Pollutant

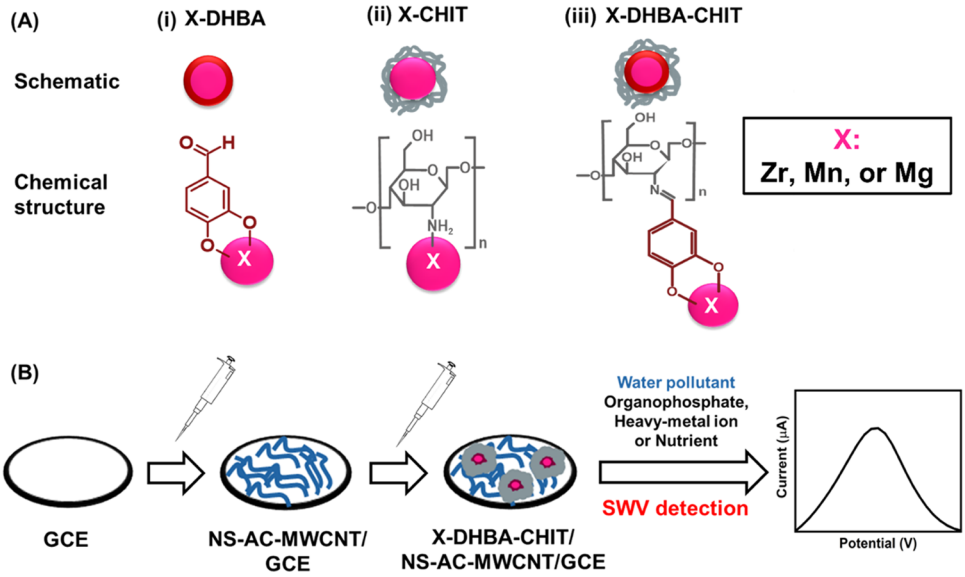

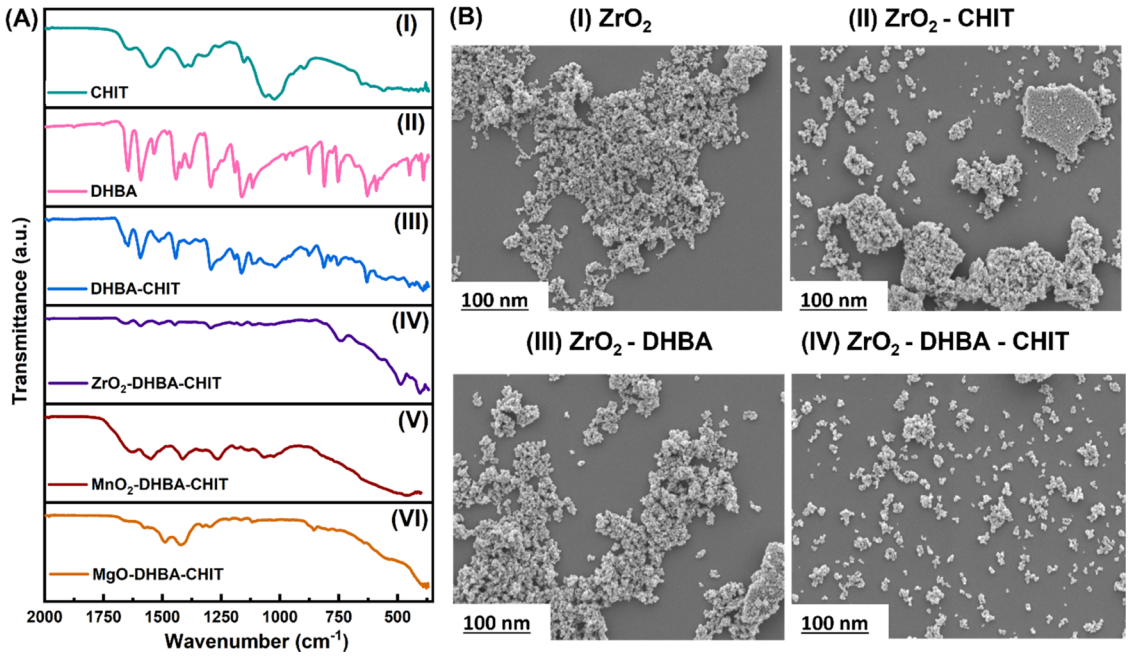

Figure 1. (A) FTIR spectra for (I) as-received CHIT; (II) as-received DHBA; (III) DHBA-modified CHIT; DHBA-CHIT modification of (IV) ZrO_2, (V) MnO_2, and (VI) MgO. (B) SEM images of (I) as-received ZrO_2 and ZrO_2 modified with (II) CHIT, (III) DHBA, and (IV) DHBA-CHIT.

ZrO_2, ZrO_2-CHIT, ZrO_2-DHBA, and ZrO_2-DHBA-CHIT were prepared. For MnO_2, surface modification was accomplished with aqueous suspensions of bare MnO_2 and MnO_2-DHBA-CHIT. A similar procedure was employed for MgO surface modification. A CHIT solution of 3 g L^{-1} concentration was synthesized by dissolving CHIT using 1% acetic acid in DI water. A DHBA solution of 8 g L^{-1} was synthesized by adding DHBA to DI water. For the DHBA-CHIT solution, the CHIT solution was added to the DHBA solution with a CHIT: DHBA mass ratio of 1:2. Subsequently, surface modification of ZrO_2, MnO_2, and MgO was performed by adding these materials to the aqueous suspensions discussed above.

2.1.2. NS-AC-MWCNT Ink Synthesis. NS-AC-MWCNT is prepared with KOH activation and carbonization of polypyrrole-coated multiwalled carbon nanotubes (PPy-MWCNT).[37] The PPy-MWCNT is synthesized by chemical polymerization of pyrrole using ammonium persulfate as an oxidant and eriochrome cyanine that acts as a multifunctional dopant for Py and dispersing agent for carbon nanotubes.[38,39] The detailed synthesis procedure of PPy-MWCNT and NS-AC-MWCNT inks is discussed in our previous work.[19]

2.1.3. Sensor Fabrication. Fabrication of the electrochemical sensor is described in Scheme 1. A bare GCE is polished with 0.05 μm alumina powder and washed with DI water by ultrasonication. The NS-AC-MWCNT ink is drop-cast on the cleaned GCE and subsequently air-dried. Next, the X-DHBA-CHIT (where X denotes ZrO_2, MnO_2, or MgO) ink is printed and air-dried to produce a layer-on-layer X-DHBA-CHIT/NS-AC-MWCNT/GCE electrode. The fabricated electrodes are electrochemically pretreated by performing

https://doi.org/10.1021/acsanm.2c04105
ACS Appl. Nano Mater. XXXX, XXX, XXX−XXX

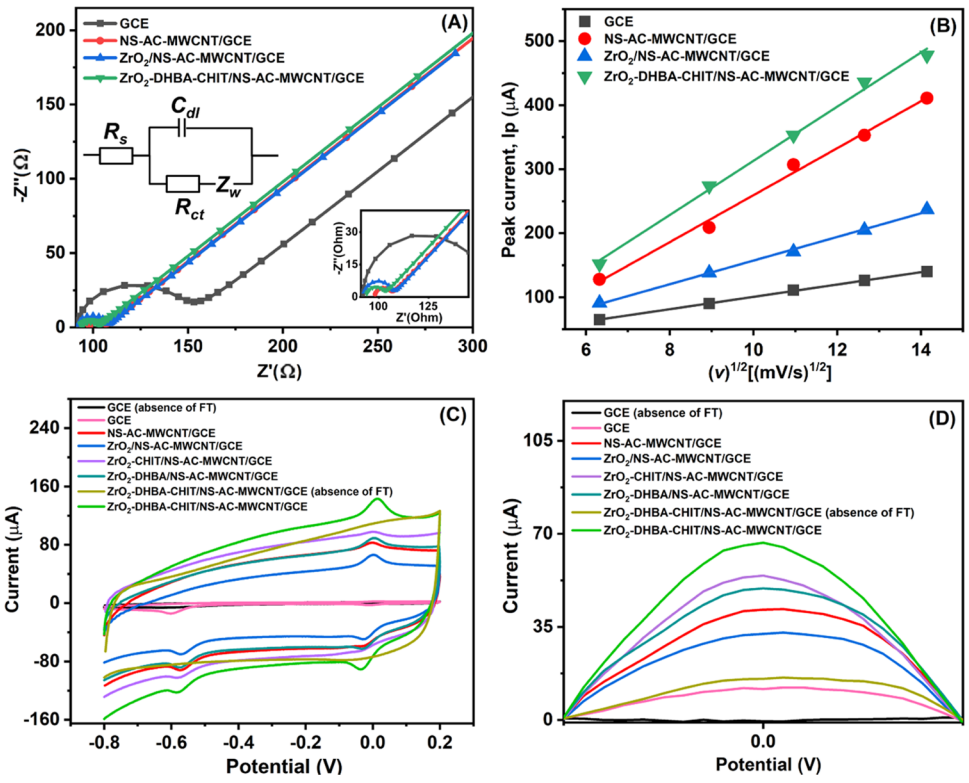

Figure 2. Fabricated electrode characterization with (A) EIS on GCE, NS-AC-MWCNT/GCE, ZrO_2/NS-AC-MWCNT/GCE, and ZrO_2-DHBA-CHIT/NS-AC-MWCNT/GCE electrodes in 0.5 mM $Fe(CN)_6^{3-}/Fe(CN)_6^{4-}$ and 0.1 M KCl in 10^{-1} to 10^5 Hz (5 mV). (B) Peak current vs square root of scan rate plots for electroactive surface area evaluation of GCE, NS-AC-MWCNT/GCE, ZrO_2/NS-AC-MWCNT/GCE, and ZrO_2-DHBA-CHIT/NS-AC-MWCNT/GCE electrodes for scan rates 0.04−0.2 V s^{-1} for 20 μM FT in pH 5 buffer solution. (C) CV and (D) SWV study of GCE (FT-deprived), GCE, NS-AC-MWCNT, ZrO_2/NS-AC-MWCNT/GCE, ZrO_2-CHIT/NS-AC-MWCNT/GCE, ZrO_2-DHBA/NS-AC-MWCNT/GCE, and ZrO_2-DHBA-CHIT/NS-AC-MWCNT/GCE in 20 μM FT (pH 5, 0.05 V s^{-1} scan rate).

CV from 0.1 to 1.2 V in ABS that has a pH = 5 at 0.1 V s^{-1}. Electrochemical sensing is performed with CV and SWV. The CVs are conducted in 0.2 M pH = 5 ABS from −0.8 to 0.2 V for FT, −1.0 to −0.4 V for Pb^{2+}, and 0−1.1 V vs Ag/AgCl for NO_2^- at 0.05 V s^{-1} scan rate. Electroactive surface area characterization of the electrodes is also performed with CV in 0.5 mM $Fe(CN)_6^{3-}/Fe(CN)_6^{4-}$/0.1 M KCl at scan rates ranging from 0.04 to 0.2 V s^{-1}. The fabricated sensor is optimized for FT detection with SWV. The limit of detection (LOD) of the ZrO_2-DHBA-CHIT/NS-AC-MWCNT/GCE sensor for FT is calculated through the relationship $3\sigma/m$, where σ denotes the standard deviation of the SWV response for blank samples and m denotes the slope of the calibration curve for FT-containing samples. Specificity of the ZrO_2-DHBA-CHIT/NS-AC-MWCNT/GCE sensor toward FT is examined using a 20-fold excess concentration of several frequently found chemical interferents. A recovery study in ABS (0.2 M, pH 5) is performed with lake water (filtered with 8 μm pore size filter paper) and tap water.

3. RESULTS AND DISCUSSION

3.1. Material Characterization. We use Fourier transform infrared spectroscopy (FTIR) to investigate the modification of bare ZrO_2, MnO_2, and MgO surfaces with DHBA-modified CHIT. DHBA modification with CHIT is studied first, followed by immobilization of inorganic oxides. As seen in Figure 1A, as-received CHIT powder exhibits characteristic absorptions at ∼1550, 1062, and 1024 cm^{-1}, indicating the presence of amide II, primary −OH, and C−O−C groups.[40,41] The 1062 cm^{-1} absorption peak is found shifted to 1077 cm^{-1} in ZrO_2-CHIT spectra (Figure S1), revealing potential interaction between ZrO_2 and the hydroxyl group of CHIT. Synthesis of DHBA-modified CHIT is confirmed by the C═N bond formed between the aldehyde group of DHBA and the amino group of CHIT via the Schiff base reaction.[33,42] Corresponding absorptions of the C═N bond are found in DHBA-CHIT (∼1642 cm^{-1}), ZrO_2-DHBA-CHIT (∼1650 cm^{-1}), MnO_2-DHBA-CHIT (∼1635 cm^{-1}), and MgO-DHBA-CHIT (∼1649 cm^{-1}) spectra implying Schiff base formation. The ZrO_2-DHBA-CHIT spectra showed stretching vibrations at ∼748 and 485 cm^{-1} for Zr−O in ZrO_2[43,44] and a sharp peak at 450 cm^{-1} for Zr−O−Zr linkage.[45] Another sharp peak at ∼1384 cm^{-1} indicative of the −OH group of DHBA[41] does not appear for ZrO_2-DHBA-CHIT but does for DHBA-CHIT and DHBA, possibly due to bidentate bonding of DHBA to surface ZrO_2 nanoparticles (as shown in Scheme S1). This confirms the surface modification of ZrO_2 nanoparticles with DHBA-modified CHIT. Similarly, the ∼1384 cm^{-1} peak does not appear in the MnO_2-DHBA-CHIT and MgO-DHBA-CHIT spectra, confirming the surface modification of both MnO_2 and MgO with DHBA-CHIT. Finally, the MnO_2-DHBA-CHIT spectra reveal a broad peak at 460 cm^{-1} attributed to Mn−O vibration[46] and MgO-DHBA-CHIT spectra absorptions at 643 and ∼550 cm^{-1} ascribed to Mg−O vibrations.[47]

ZrO_2 surface modification by CHIT, DHBA, and DHBA-CHIT is investigated with SEM. Unmodified ZrO_2 nanoparticles reveal heavy agglomeration (Figure 1B(I)) since they do not bond strongly to the substrate. CHIT modification of the nanoparticles promotes this agglomeration (Figure 1B-B(II)). In contrast, DHBA-modified ZrO_2 nanoparticles (Figure 1B(III)) produce more surface coverage and fewer

https://doi.org/10.1021/acsanm.2c04105
ACS Appl. Nano Mater. XXXX, XXX, XXX−XXX

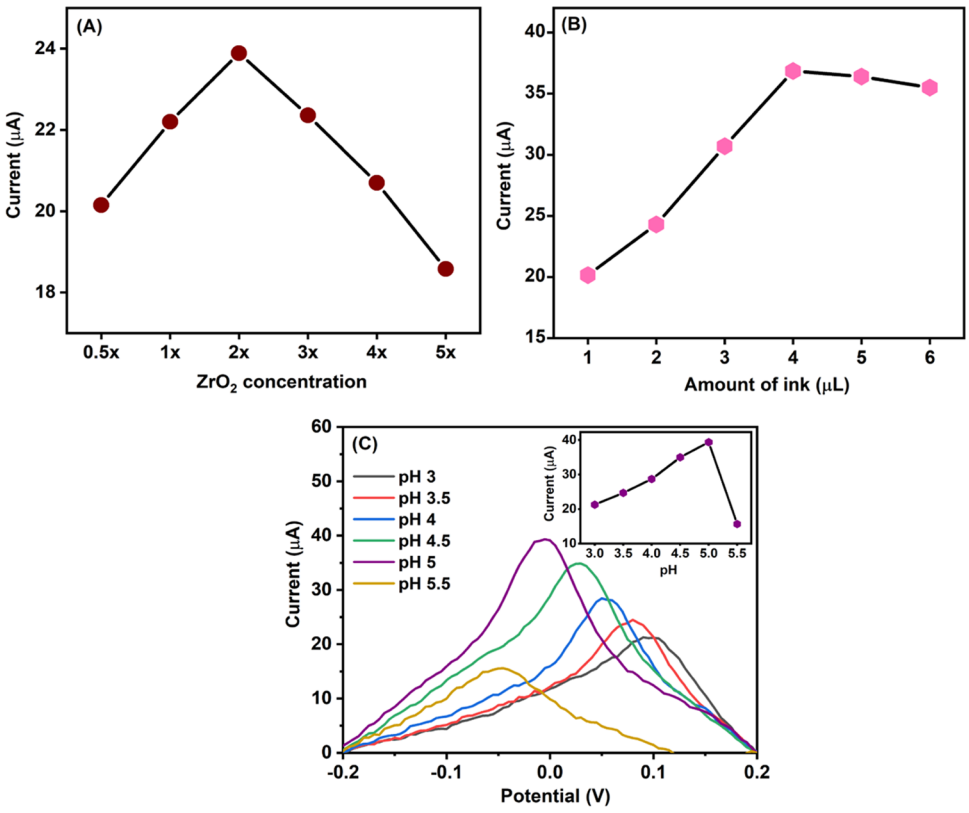

Figure 3. SWV-assisted optimization study of (A) ZrO_2 concentration in the ZrO_2-DHBA-CHIT matrix for 20 μM FT (pH 5), (B) amount of ZrO_2-DHBA-CHIT ink deposition on NS-AC-MWCNT/GCE for 20 μM FT (pH 5), and (C) pH of the buffer solution in 3−5.5 pH range for 20 μM FT.

agglomerates on a silicon substrate, behavior that is enhanced by DHBA-CHIT modification of ZrO_2 nanoparticles (Figure 1B(IV)). Moreover, SEM images of DHBA-CHIT-modified MnO_2 and MgO (Figure S2) reveal uniform surface coverage with even films. The more even and uniform surface coverage of the substrates is attributed to the strong DHBA-assisted immobilization of nanoparticles on the surface and the film-forming properties of CHIT.

Electrochemical impedance spectroscopy (EIS) is employed to investigate the influence of surface modification of ZrO_2 nanoparticles with DHBA-CHIT by comparing the charge transfer resistance of modified ZrO_2 against unmodified ZrO_2 nanoparticles and different electrode fabricating materials (Figure 2A). A Randles equivalent circuit is used to model and fit the impedance data and generate Nyquist plots.[48] The charge transfer resistance of the electrode (R_{ct}) represents the ease of electron transfer at the electrode−electrolyte interface.

As expected, Figure 2A shows that modification of GCE with NS-AC-MWCNT decreases the charge transfer resistance of an electrode from R_{ct} (GCE) = 53.7 Ω to R_{ct} (NS-AC-MWCNT/GCE) = 7.7 Ω. This is attributed to the superior electrical conductivity and electroactive surface area of NS-AC-MWCNT over bare GCE.[19] Deposition of unmodified ZrO_2 nanoparticles on NS-AC-MWCNT/GCE increases R_{ct} to 14 Ω, which is likely due to nanoparticle agglomeration on the electrode surface, which reduces the available electroactive surface area of the working electrode. Immobilization of the modified ZrO_2 nanoparticles with DHBA-CHIT on NS-AC-MWCNT/GCE shows a significant decrease in R_{ct} to 8.3 Ω as compared to the value for ZrO_2/NS-AC-MWCNT/GCE, indicating considerable enhancement of ZrO_2 nanoparticle immobilization through stronger bonding between nanoparticles and the electrode surface. The reduction in nanoparticle agglomeration enhances the surface area of the electrode available for electrochemistry. R_{ct} for the modified ZrO_2-DHBA-CHIT/NS-AC-MWCNT/GCE is higher than that for NS-AC-MWCNT/GCE, likely due to the lower electrical conductivity of CHIT.

CV is used to collect the electrochemical response of different electrodes, and the Randles−Sevcik equation[49] is employed to calculate the electroactive surface area. Graphs of the anodic peak current (I_p) vs square root of the scan rate ($\nu^{1/2}$) are plotted (Figure 2B), and their slopes are used to determine the surface area.

$$I_p = 2.69 \times 10^5 n^{3/2} A C D^{1/2} \nu^{1/2}$$

, where n represents the number of participating electrons, A is the electroactive surface area of the electrode, and C and D are the concentration and diffusion coefficient of $Fe(CN)_6^{3-}$/$Fe(CN)_6^{4-}$, respectively. The scan rate is varied from 0.04 to 0.2 V s^{-1}. The surface areas thus determined are 0.028, 0.109, 0.055, and 0.126 cm^2 for GCE, NS-AS-MWCNT/GCE, ZrO_2/NS-AC-MWCNT/GCE, and ZrO_2-DHBA-CHIT/NS-AC-MWCNT/GCE, respectively. NS-AS-MWCNT modification of GCE increases the surface area almost 4-fold. Modification of NS-AC-MWCNT/GCE with unmodified ZrO_2 nanoparticles reduces the surface area compared with NS-AC-MWCNT/GCE, indicating formation of nanoparticles agglomerates. Conversely, deposition of ZrO_2 modified with DHBA-CHIT on NS-AC-MWCNT/GCE provides the highest electroactive surface area, a 4.5-fold increase relative to GCE.

https://doi.org/10.1021/acsanm.2c04105
ACS Appl. Nano Mater. XXXX, XXX, XXX−XXX

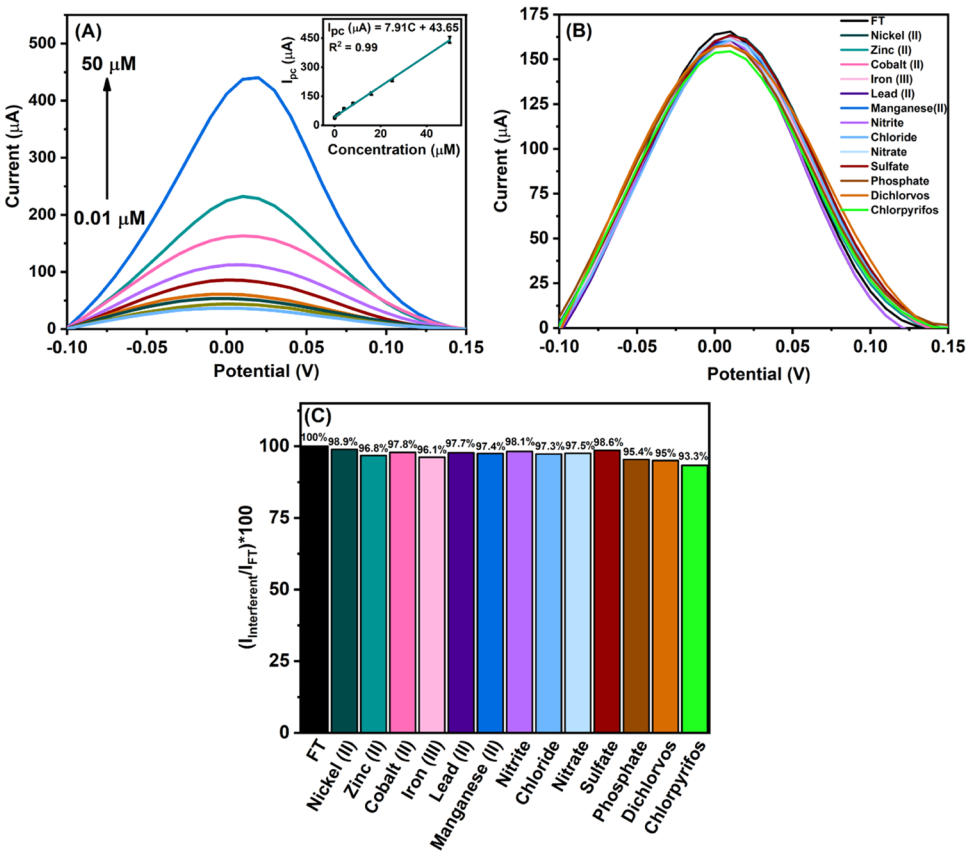

Figure 4. (A) Sensor performance of ZrO_2-DHBA-CHIT/NS-AC-MWCNT/GCE for FT concentrations in 0.01−50 μM range (pH 5); inset represents the calibration plot of peak current vs FT concentration. Number of replicates, n = 3. (B, C) Interference study of the ZrO_2-DHBA-CHIT/NS-AC-MWCNT/GCE sensor with 20-fold concentrations of commonly found chemical interferents in consuming water in 20 μM FT (pH 5).

We suggest that CHIT enhances film formation of the composite and DHBA supports nanoparticle distribution by reducing agglomeration, thus enhancing the available surface area for the working electrode.

Further electrochemical characterization of the fabricated electrodes is performed with their CV and SWV responses for FT detection (Figure 2C,D). The redox-active nitro group of FT produces an irreversible reduction, quasi-reversible oxidation, and reduction peaks during forward and reverse CV scans.[19,50] Similar characteristic peaks are observed for FT detection with all of the working electrodes (Figure 2C,D). CV and SWV profiles of the electrodes are compared with their faradic current response. The NS-AC-MWCNT-modified GCE electrode considerably improves the faradic current response as compared to GCE due to its superior electrocatalytic properties. Deposition of unmodified ZrO_2 nanoparticles as the FT-detecting agent on the NS-AC-MWCNT/GCE shows a decrease in current in CV and SWV response. This result is supported by EIS and electrochemical surface area studies. However, deposition of CHIT-modified ZrO_2 on NS-AC-MWCNT/GCE reveals an increase in the current response compared to that on NS-AC-MWCNT/GCE. This occurs due to interaction between CHIT and ZrO_2, as observed through the FTIR study, thereby facilitating the charge transfer between FT and the electrode. An even better current response is noted with DHBA-modified ZrO_2/NS-AC-MWCNT/GCE, mainly due to the addition of the redox activity of DHBA[51,52] in the composite and improved nanoparticle dispersion. DHBA-CHIT-linked ZrO_2 on NS-AC-MWCNT/GCE has the highest faradic current response among all electrodes due to the synergetic effect of well-dispersed ZrO_2 nanoparticles and NS-AC-MWCNT. Thus, for this case, synergetic enhancement of electrochemical surface area, the electrical conductivity of the electrode, and the strong affinity for the phosphoric group (of FT) considerably improve the current response for FT detection.

3.2. Sensor Optimization. The optimal concentration of ZrO_2 for the DHBA-modified CHIT is evaluated through the electrode SWV response for FT detection. The concentration of ZrO_2 is varied from 0.5x to 5x (with x = 33.3 g L^{-1}), with concentrations of DHBA and CHIT held constant. The current response increases with increasing ZrO_2 concentration up to 2x (Figure 3A) because of the greater availability of nanoparticles in the DHBA-CHIT matrix. Further increase in ZrO_2 concentration results in a decrement in current response since enough DHBA-CHIT ligands are no longer available to link ZrO_2 nanoparticles. This encourages nanoparticle agglomeration and reduces the electrocatalytic properties of the electrode. Thus, 2x is an optimal concentration for ZrO_2 in DHBA-modified CHIT. Next, the optimal ZrO_2-DHBA-CHIT ink deposition on NS-AC-MWCNT/GCE is evaluated. As seen in Figure 3B, the current response increases from 1 to 4 μL but does not increase thereafter with further increase in ink deposition after the electrode surface coverage has been maximized. Hence, 4 μL is chosen as the optimal deposition volume for the ZrO_2-DHBA-CHIT ink.

https://doi.org/10.1021/acsanm.2c04105
ACS Appl. Nano Mater. XXXX, XXX, XXX−XXX

Table 1. Comparison of Modified Electrodes for Electrochemical Detection of FT

electrode	mechanism	technique	linear range (μM)	LOD (nM)	refs
ZrO_2-DHBA-CHIT/NS-AC-MWCNT/GCE	nonenzymatic	SWV	0.010−50.0	1.69	this work
1T-WS_2/GA/AChE-BSA/GCE	enzymatic	chronoamperometry	0.001−1.0	2.86	23
Tyr/poly(2-hydroxybenzamide)/GE	enzymatic	amperometry	0.018−3.60	4.7	53
NS-AC-MWCNT/GCE	nonenzymatic	SWV	0.050−40.0	4.91	19
ZrO_2/rGO/MoS_2-Au/GCE	nonenzymatic	SWV	0.018−21.6	7.94	24
AuNPs@GNIP-GR-IL/GCE	nonenzymatic	DPV[a]	0.010−5.0	8.0	54
MWCNT/GCE	nonenzymatic	SWV	0.20−60.0	80.0	55

[a]AChE, acetylcholinesterase; Tyr, tyrosinase; DPV, differential pulse voltammetry.

The pH of the acetate buffer solution is similarly varied from 3 to 6 to assess electrode performance for FT detection. The current response increases with pH increases from 3 to 5, followed by a decrease with further increases in pH (Figure 3C). This is attributed to the increased proton concentration due to reduction of the FT NO group. The proton concentration decreases with increasing pH, which limits NO reduction and thus current response. Therefore, pH = 5 is selected for the acetate buffer solution as being optimal. Next, we consider the adsorption-controlled FT detection facilitated by the affinity of ZrO_2 for the phosphoric group and effects of accumulation potential (a_p) and time (a_t) on current response. We vary a_p from −0.8 to −0.5 V (vs Ag/AgCl) for a_t = 25 s with magnetic stirring. The peak current increases with decreasing a_p until −0.6 V (Figure S3A), but a further decrease in a_p now decreases the peak current. Subsequently, we hold a_p = −0.6 V and vary a_t between 25 and 150 s. The highest current response occurs at 100 s and saturates with further increases in a_t (Figure S3B). Consequently, a_p of −0.6 V potential for 100 s is selected as optimal for SWV detection of FT.

Sensor optimization is also performed by examining the SWV parameters, such as frequency, step potential, and amplitude, which are varied to obtain the optimal peak current shape and highest current response for FT detection. The frequency is analyzed by varying it from 5 to 25 Hz with constant step potential and amplitude of 5 and 50 mV, respectively. The peak current increases to 10 Hz, followed by a decrease (Figure S4A) based on which a 10 Hz frequency is selected. Next, the step potential is varied from 3 to 20 mV at 10 Hz (Figure S4B), where 10 mV is selected as optimal considering the peak shape and current response. Finally, the amplitude is examined by varying it between 40 and 180 mV. As shown in Figure S4C, the highest current response occurs at 140 mV, which is selected as optimal at a 10 Hz frequency and 10 mV step potential for SWV detection of FT.

3.3. Sensor Performance. An analytical determination of sensitivity is performed for the ZrO_2-DHBA-CHIT/NS-AC-MWCNT/GCE sensor for different FT concentrations under the optimized conditions. The current response for different concentrations ranging from 50 to 0.01 μM is used to plot the calibration curve (Figure 4A), which provides the linear relation I_{pc} (μA) = 7.91C (μM) + 26.38 with R^2 = 0.99. The limit of detection is 1.69 nM, which is calculated from the relation $3\sigma/m$, where σ denotes the standard deviation of the SWV response for blank samples and m denotes the slope of the calibration curve with three replicates per FT concentration.

The sensor performance exceeds that for enzymatic-based sensors (Table 1) for FT detection. This is because ZrO_2 nanoparticles are better dispersed through DHBA-CHIT chemistry, increasing the electrode electroactive surface area and enhancing FT capture. The improved redox activity from DHBA in the composite increases charge transfer through the modified electrode. In addition, NS-AC-MWCNT as the supporting electrode improves electrocatalysis due to its higher electrical conductance and surface area.[19] Thus, the synergistic effect of ZrO_2 nanoparticles and NS-AC-MWCNT enhances the overall signal response during FT detection.

The specificity of a sensor is a critical characteristic since it must be agnostic to chemical interfering agents contained in environmental samples. Since ZrO_2 has affinity toward phosphate,[5] we attribute the specificity of the ZrO_2-DHBA-CHIT/NS-AC-MWCNT/GCE electrode toward FT to covalent bonding between Zr and the phosphate group of FT, as illustrated in Scheme S2. We spike drinking water with interferent agents in 20-fold excess concentrations (320 μM) relative to FT (16 μM). All interferents, apart from phosphate, chlorpyrifos, and dichlorvos, have a negligible influence on FT detection (Figure 4B,C) by the ZrO_2-DHBA-CHIT/NS-AC-MWCNT/GCE sensor due to the behavior of ZrO_2 as a detecting agent for the analyte, i.e., FT. The minor influence of phosphate occurs because of the ZrO_2 affinity toward phosphate. The relative lack of response to the chlorpyrifos and dichlorvos interferents for this sensor is better than that for the one fabricated with NS-AC-MWCNT/GCE[19] due to the ZrO_2-DHBA-CHIT coating on NS-AC-MWCNT/GCE, which reduces $\pi-\pi$ interactions of the sensor with chlorpyrifos. Therefore, incorporating ZrO_2 as the detecting agent in the NS-AC-MWCNT/GCE composite improves selectivity toward FT.

Sensor utilization in lake and tap water, its stability at room temperature and 4 °C, and repeatability are also examined. Tap water and filtered lake water are spiked with 16, 8, and 4 μM FT concentrations determined with the generated calibration curve. Table 2 shows that the sensor recovers spiked FT concentrations in the range 91.9−97.5% with RSD 4.6−5.5% in lake water and 93.8−98.8% with RSD 3.8−5.5% in tap water. The recovery performance in lake water is slightly lower

Table 2. FT Recovery in Lake and Tap Water for 16, 8, and 4 μM Concentrations (pH 5) with Three Replicates Per Concentration

water sample	spiked FT (μM)	found FT (μM)	recovery (%)
lake water	16	15.61 ± 0.84	97.5 ± 5.4
	8	7.74 ± 0.36	96.7 ± 4.6
	4	3.67 ± 0.2	91.9 ± 5.5
tap water	16	15.79 ± 0.59	98.6 ± 3.7
	8	7.9 ± 0.38	98.8 ± 4.8
	4	3.75 ± 0.2	93.8 ± 5.5

https://doi.org/10.1021/acsanm.2c04105
ACS Appl. Nano Mater. XXXX, XXX, XXX−XXX

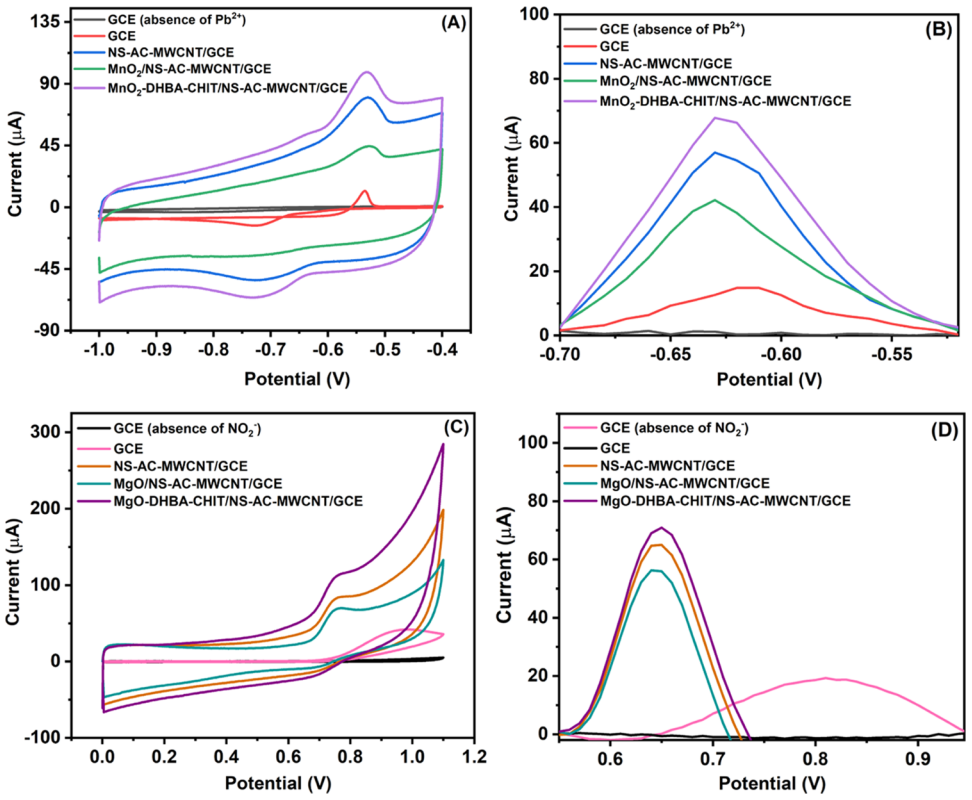

Figure 5. (A, B) CV and SWV detection of 20 μM Pb^{2+} at GCE (absence of Pb^{2+}), GCE, NS-AC-MWCNT/GCE, MnO_2/NS-AC-MWCNT/GCE, and MnO_2-DHBA-CHIT/NS-AC-MWCNT/GCE in ABS (pH 5). (C, D) CV and SWV response for 20 μM NO_2^- at GCE (absence of NO_2^-), GCE, NS-AC-MWCNT/GCE, MgO/NS-AC-MWCNT/GCE, and MgO-DHBA-CHIT/NS-AC-MWCNT/CGE in ABS (pH 5). The scan rate of CV is 0.05 V s^{-1}.

due to the passivation of the electrode surface with more waste, or contamination, in lake water. The antifouling ability of the fabricated sensor tested in the lake water is markedly superior compared to the NS-AC-MWCNT/GCE sensor. The LOD measurements are performed for both the sensors with several FT concentrations, ranging from 20 to 2 μM in lake water (Figure S5). For the ZrO_2-DHBA-CHIT/NS-AC-MWCNT/GCE sensor, LOD = 11.3 nM compared to 19.8 nM for NS-AC-MWCNT/GCE. The improvement in the antifouling ability of the ZrO_2-DHBA-CHIT/NS-AC-MWCNT/GCE sensor is attributed to the enhancement in target species capture with ZrO_2. A uniform DHBA-CHIT-assisted coating blocks interferent access to the surface of the conductive electrode. The sensor is stable at both room temperature and under refrigeration for at least 4 weeks. Storage of the sensor at room temperature and 4 °C for 4 weeks has virtually no influence on FT detection (for the 16 μM sample), where the sensor recovers 94.3 and 96.6% current responses as compared to the initial response, respectively (Figure S6). The RSD for all FT concentrations is lower than 4.9%, demonstrating excellent repeatability.

Other water pollutants can also be detected using the same DHBA-CHIT method for immobilized inorganic oxides with affinity toward the analyte. We modified the MnO_2 surface with DHBA-CHIT and deposited it on NS-AC-MWCNT/GCE to detect Pb^{2+} ions in an aqueous solution. MnO_2 has affinity toward Pb^{2+} ions due to electrostatic interactions,[25] leading to involvement of potential electrostatic interactions between negatively charged MnO_2 and Pb^{2+} ions. We suggest that these interactions impart the specificity and enhance charge transfer capabilities of the MnO_2-DHBA-CHIT/NS-AC-MWCNT/GCE electrode. CV and SWV were employed to analyze electrode electrochemical performances to detect 20 μM Pb^{2+} in pH 5 ABS. The CV reveals anodic and cathodic peaks at ∼−0.53 and ∼−0.72 V vs Ag/AgCl, respectively, in the −1 to −0.4 V potential range vs Ag/AgCl (Figure 5A).[56] The SWV reveals a characteristic peak at ∼−0.62 V vs Ag/AgCl (Figure 5B). Both CV and SWV studies indicate faradic current responses in increasing order as follows for the electrodes: GCE < MnO_2/NS-AC-MWCNT/GCE < NS-AC-MWCNT/GCE < MnO_2-DHBA-CHIT/NS-AC-MWCNT/GCE. The highest current response to detect Pb^{2+} is for MnO_2-DHBA-CHIT/NS-AC-MWCNT/GCE. The detecting agent MnO_2 enhances the surface area of the electrode and significantly enhances Pb^{2+} adsorption on the electrode, providing an example of the application of DHBA-CHIT to fabricate a MnO_2-surface-modified NS-AC-MWCNT/GCE sensor that detects heavy-metal ions.

Since MgO nanoparticles have affinity toward nitrite (NO_2^-) ions due to electron transfer and acid−base-like interactions,[26] we suggest that these interactions facilitate the specific and sensitive electrochemical responses of the MgO-DHBA-CHIT/NS-AC-MWCNT/GCE electrochemical sensor for NO_2^- detection. CV and SWV are performed for this sensor with 20 μM NO_2^- in pH 5 ABS in the potential range from 0 to 1.1 V vs Ag/AgCl. As shown in Figure 5C,D, the CV reveals an oxidation peak at ∼0.75 V (vs Ag/AgCl), and the SWV has a characteristic oxidation peak at ∼0.65 V (vs Ag/AgCl) for all electrodes except GCE.[57] The broad oxidation peak for NO_2^- with GCE at a higher potential occurs due to

https://doi.org/10.1021/acsanm.2c04105
ACS Appl. Nano Mater. XXXX, XXX, XXX−XXX

slower reaction kinetics and limited analyte diffusion across the bare electrode. The MgO-DHBA-CHIT/NS-AC-MWCNT/GCE electrode shows the highest current response toward NO_2^- ions. As discussed, incorporation of the inorganic oxide into the NS-AC-MWCNT/GCE composite with the DHBA-CHIT method enhances the available surface area, analyte capture, and charge transfer of the electrode. For optimal performance from MgO-DHBA-CHIT/NS-AC-MWCNT/GCE and MnO_2-DHBA-CHIT/NS-AC-MWCNT/GCE, each sensor's parameter must be optimized. Besides, the preliminary results of the methodology indicate that this platform can be used to modify other metal oxides or metals for fabricating highly sensitive sensors.

4. CONCLUSIONS

Uniformly coated, stable, and highly electrocatalytic electrodes are fabricated as ultrasensitive nonenzymatic electrochemical sensors for specific detection of water pollutants. A detecting agent with high affinity for the analyte is incorporated into the electrode modifying ink using the catechol molecule 3,4-dihydroxybenzaldehyde (DHBA) and polymer chitosan (CHIT). A simple and effective method immobilizes metal oxides through strong adsorption by DHBA and film formation with CHIT. The detecting agents ZrO_2, MnO_2, and MgO have specific affinities to fenitrothion (FT, an organophosphate), lead (Pb^{2+}, a heavy-metal ion), and nitrite (NO_2^-, a nutrient), respectively. Surface modification with these metal oxides enhances electronic and film-forming properties of electrodes that increase the total surface area. We drop-cast X-DHBA-CHIT (X: ZrO_2, MnO_2, or MgO) ink on the glassy carbon electrode (GCE) modified with nitrogen−sulfur codoped activated carbon-coated carbon nanotubes (NS-AC-MWCNT). The X-DHBA-CHIT and NS-AC-MWCNT work synergistically to enhance the electrocatalytic properties of the electrode. As a result, the ZrO_2-DHBA-CHIT/NS-AC-MWCNT/GCE sensor produces an excellent current response for FT detection. With a 1.69 nM detection limit, the sensor reliably detects FT in lake and tap water due to its excellent antifouling properties. The sensor is stable for 4 weeks at room temperature and when stored at 4 °C and experiences negligible influence from chemical interferents. The current responses of MnO_2-DHBA-CHIT/NS-AC-MWCNT/GCE and MgO-DHBA-CHIT/NS-AC-MWCNT/GCE electrodes have excellent detection capabilities for Pb^{2+} and NO_2^-, respectively. For the optimal performance from MnO_2- and MgO-modified electrodes, each electrochemical parameter must be optimized.

■ ASSOCIATED CONTENT

Supporting Information

The Supporting Information is available free of charge at https://pubs.acs.org/doi/10.1021/acsanm.2c04105.

FTIR characterization of CHIT and ZrO_2-CHIT; schematic of metal oxide adsorption mechanisms with DHBA; optimization of accumulation potential and time; SWV (frequency, step potential, and amplitude); schematic of interaction between Zr and FT; LOD measurements in lake water; and sensor's 4 week storage response for FT detection (PDF)

■ AUTHOR INFORMATION

Corresponding Author

Ishwar K. Puri − *Department of Engineering Physics, McMaster University, Hamilton, Ontario L8S 4L8, Canada; Department of Aerospace and Mechanical Engineering, University of Southern California, Los Angeles, California 90089, United States;* orcid.org/0000-0002-8713-4188; Email: ikpuri@mcmaster.ca

Authors

Krishna Jangid − *Department of Engineering Physics, McMaster University, Hamilton, Ontario L8S 4L8, Canada;* orcid.org/0000-0003-3603-3982

Rakesh P. Sahu − *Department of Mechanical Engineering and Department of Materials Science and Engineering, McMaster University, Hamilton, Ontario L8S 4L8, Canada;* orcid.org/0000-0003-2443-6741

Sadman Sakib − *Department of Engineering Physics, McMaster University, Hamilton, Ontario L8S 4L8, Canada;* orcid.org/0000-0001-7601-6680

Igor Zhitomirsky − *Department of Materials Science and Engineering, McMaster University, Hamilton, Ontario L8S 4L8, Canada*

Complete contact information is available at: https://pubs.acs.org/10.1021/acsanm.2c04105

Notes

The authors declare no competing financial interest.

■ ACKNOWLEDGMENTS

This work was supported by the Natural Sciences and Engineering Research Council of Canada (NSERC) Discovery Grant (RGPIN-2019-06571). The authors thank Christopher Butcher of Canadian Centre for Electron Microscopy for SEM.

■ REFERENCES

(1) Carolin, C. F.; Kumar, P. S.; Saravanan, A.; Joshiba, G. J.; Naushad, M. Efficient techniques for the removal of toxic heavy metals from aquatic environment: A review. *J. Environ. Chem. Eng.* **2017**, *5*, 2782−2799.

(2) Zamora-Ledezma, C.; Negrete-Bolagay, D.; Figueroa, F.; Zamora-Ledezma, E.; Ni, M.; Alexis, F.; Guerrero, V. H. Heavy metal water pollution: A fresh look about hazards, novel and conventional remediation methods. *Environ. Technol. Innovation* **2021**, *22*, No. 101504.

(3) Bolat, G.; Abaci, S.; Vural, T.; Bozdogan, B.; Denkbas, E. B. Sensitive electrochemical detection of fenitrothion pesticide based on self-assembled peptide-nanotubes modified disposable pencil graphite electrode. *J. Electroanal. Chem.* **2018**, *809*, 88−95.

(4) Schierenbeck, T. M.; Smith, M. C. Path to impact for autonomous field deployable chemical sensors: a case study of in situ nitrite sensors. *Environ. Sci. Technol.* **2017**, *51*, 4755−4771.

(5) Liu, G.; Lin, Y. Electrochemical sensor for organophosphate pesticides and nerve agents using zirconia nanoparticles as selective sorbents. *Anal. Chem.* **2005**, *77*, 5894−5901.

(6) Cabral Pinto, M. M. S.; Marinho-Reis, P.; Almeida, A.; Pinto, E.; Neves, O.; Inácio, M.; Gerardo, B.; Freitas, S.; Simões, M. R.; Dinis, P. A.; et al. Links between cognitive status and trace element levels in hair for an environmentally exposed population: A case study in the surroundings of the estarreja industrial area. *Int. J. Environ. Res. Public Health* **2019**, *16*, No. 4560.

(7) Lin, B.; Xu, J.; Lin, K.; Li, M.; Lu, M. Low-cost automatic sensor for in situ colorimetric detection of phosphate and nitrite in agricultural water. *ACS Sens.* **2018**, *3*, 2541−2549.

https://doi.org/10.1021/acsanm.2c04105
ACS Appl. Nano Mater. XXXX, XXX, XXX−XXX

(8) Li, X.; Ping, J.; Ying, Y. Recent developments in carbon nanomaterial-enabled electrochemical sensors for nitrite detection. *TrAC, Trends Anal. Chem.* **2019**, *113*, 1−12.
(9) Sherma, J.; Zweig, G. Pesticides. *Anal. Chem.* **1985**, *57*, 1−15.
(10) Zhang, P.; Chen, Y.-P.; Wang, W.; Shen, Y.; Guo, J.-S. Surface plasmon resonance for water pollutant detection and water process analysis. *TrAC, Trends Anal. Chem.* **2016**, *85*, 153−165.
(11) Tuan, S.-J.; Tsai, H.-M.; Hsu, S.-M.; Li, H.-P. Multiresidue analysis of 176 pesticides and metabolites in pre-harvested fruits and vegetables for ensuring food safety by gas chromatography and high performance liquid chromatography. *J. Food Drug Anal.* **2009**, *17*, 163−177.
(12) Silva, I. B.; de Araújo, D. M.; Vocciante, M.; Ferro, S.; Martínez-Huitle, C. A.; Dos Santos, E. V. Electrochemical determination of lead using a composite sensor obtained from low-cost green materials: Graphite/cork. *Appl. Sci.* **2021**, *11*, No. 2355.
(13) Barciela Alonso, M.; Prego, R. Determination of silicate, simultaneously with other nutrients (nitrite, nitrate and phosphate), in river waters by capillary electrophoresis. *Anal. Chim. Acta* **2000**, *416*, 21−27.
(14) Du, D.; Ye, X.; Zhang, J. Cathodic electrochemical analysis of methyl parathion at bismuth-film-modified glassy carbon electrode. *Electrochim. Acta* **2008**, *53*, 4478−4484.
(15) Gan, N.; Yang, X.; Xie, D.; Wu, Y.; Wen, W. A disposable organophosphorus pesticides enzyme biosensor based on magnetic composite nano-particles modified screen printed carbon electrode. *Sensors* **2010**, *10*, 625−638.
(16) Yang, S.; Liu, J.; Zheng, H.; Zhong, J.; Zhou, J. Simulated revelation of the adsorption behaviours of acetylcholinesterase on charged self-assembled monolayers. *Nanoscale* **2020**, *12*, 3701−3714.
(17) Liu, X.; Cheng, H.; Zhao, Y.; Wang, Y.; Li, F. Portable electrochemical biosensor based on laser-induced graphene and MnO2 switch-bridged DNA signal amplification for sensitive detection of pesticide. *Biosens. Bioelectron.* **2022**, *199*, No. 113906.
(18) Wu, J.; Yang, Q.; Li, Q.; Li, H.; Li, F. Two-dimensional MnO2 nanozyme-mediated homogeneous electrochemical detection of organophosphate pesticides without the interference of H2O2 and color. *Anal. Chem.* **2021**, *93*, 4084−4091.
(19) Jangid, K.; Sahu, R. P.; Pandey, R.; Chen, R.; Zhitomirsky, I.; Puri, I. K. Multiwalled Carbon Nanotubes Coated with Nitrogen−Sulfur Co-Doped Activated Carbon for Detecting Fenitrothion. *ACS Appl. Nano Mater.* **2021**, *4*, 4781−4789.
(20) Canevari, T. C.; Prado, T. M.; Cincotto, F. H.; Machado, S. A. Immobilization of ruthenium phthalocyanine on silica-coated multi-wall partially oriented carbon nanotubes: Electrochemical detection of fenitrothion pesticide. *Mater. Res. Bull.* **2016**, *76*, 41−47.
(21) Arduini, F.; Cinti, S.; Scognamiglio, V.; Moscone, D. Nanomaterials in electrochemical biosensors for pesticide detection: advances and challenges in food analysis. *Microchim. Acta* **2016**, *183*, 2063−2083.
(22) Yang, Y.; Asiri, A. M.; Du, D.; Lin, Y. Acetylcholinesterase biosensor based on a gold nanoparticle−polypyrrole−reduced graphene oxide nanocomposite modified electrode for the amperometric detection of organophosphorus pesticides. *Analyst* **2014**, *139*, 3055−3060.
(23) Nasir, M. Z. M.; Mayorga-Martinez, C. C.; Sofer, Z.; Pumera, M. Two-dimensional 1T-phase transition metal dichalcogenides as nanocarriers to enhance and stabilize enzyme activity for electrochemical pesticide detection. *ACS Nano* **2017**, *11*, 5774−5784.
(24) Qi, P.; Wang, J.; Wang, X.; Wang, X.; Wang, Z.; Xu, H.; Di, S.; Wang, Q.; Wang, X. Sensitive determination of fenitrothion in water samples based on an electrochemical sensor layered reduced graphene oxide, molybdenum sulfide (MoS2)-Au and zirconia films. *Electrochim. Acta* **2018**, *292*, 667−675.
(25) Su, Q.; Pan, B.; Wan, S.; Zhang, W.; Lv, L. Use of hydrous manganese dioxide as a potential sorbent for selective removal of lead, cadmium, and zinc ions from water. *J. Colloid Interface Sci.* **2010**, *349*, 607−612.
(26) Schneider, W. F. Qualitative differences in the adsorption chemistry of acidic (CO2, SO x) and amphiphilic (NO x) species on the alkaline earth oxides. *J. Phys. Chem. B* **2004**, *108*, 273−282.
(27) Pooja, D.; Kumar, P.; Singh, P.; Patil, S.*Sensors in Water Pollutants Monitoring: Role of Material*; Springer, 2020.
(28) Yu, X.-Y.; Liu, Z.-G.; Huang, X.-J. Nanostructured metal oxides/hydroxides-based electrochemical sensor for monitoring environmental micropollutants. *Trends Environ. Anal. Chem.* **2014**, *3*−*4*, 28−35.
(29) Sakib, S.; Bakhshandeh, F.; Saha, S.; Soleymani, L.; Zhitomirsky, I. Surface Functionalization of Metal Oxide Semiconductors with Catechol Ligands for Enhancing Their Photoactivity. *Sol. RRL* **2021**, *5*, No. 2100512.
(30) Wang, M.; Li, Z. Nano-composite ZrO2/Au film electrode for voltammetric detection of parathion. *Sens. Actuators, B* **2008**, *133*, 607−612.
(31) Wang, L.; Lei, T.; Ren, Z.; Jiang, X.; Yang, X.; Bai, H.; Wang, S. Fe3O4@ PDA@ MnO2 core-shell nanocomposites for sensitive electrochemical detection of trace Pb (II) in water. *J. Electroanal. Chem.* **2020**, *864*, No. 114065.
(32) Wang, Y.; Zhitomirsky, I. Bio-inspired catechol chemistry for electrophoretic nanotechnology of oxide films. *J. Colloid Interface Sci.* **2012**, *380*, 8−15.
(33) Clifford, A.; Pang, X.; Zhitomirsky, I. Biomimetically modified chitosan for electrophoretic deposition of composites. *Colloids Surf., A* **2018**, *544*, 28−34.
(34) Li, L.; Zeng, H. Marine mussel adhesion and bio-inspired wet adhesives. *Biotribology* **2016**, *5*, 44−51.
(35) Victorious, A.; Clifford, A.; Saha, S.; Zhitomirsky, I.; Soleymani, L. Integrating TiO2 nanoparticles within a catecholic polymeric network enhances the photoelectrochemical response of biosensors. *J. Phys. Chem. C* **2019**, *123*, 16186−16193.
(36) Sakib, S.; Pandey, R.; Soleymani, L.; Zhitomirsky, I. Surface modification of TiO2 for photoelectrochemical DNA biosensors. *Med. Devices Sens.* **2020**, *3*, No. e10066.
(37) Shi, K.; Ren, M.; Zhitomirsky, I. Activated carbon-coated carbon nanotubes for energy storage in supercapacitors and capacitive water purification. *ACS Sustainable Chem. Eng.* **2014**, *2*, 1289−1298.
(38) Zhu, Y.; Shi, K.; Zhitomirsky, I. Anionic dopant−dispersants for synthesis of polypyrrole coated carbon nanotubes and fabrication of supercapacitor electrodes with high active mass loading. *J. Mater. Chem. A* **2014**, *2*, 14666−14673.
(39) Chen, R.; Puri, I.; Zhitomirsky, I. Polypyrrole-carbon nanotube-FeOOH composites for negative electrodes of asymmetric supercapacitors. *J. Electrochem. Soc.* **2019**, *166*, No. A935.
(40) Pan, S.-k.; Wu, S.-j.; Kim, J.-m. Preparation of glucosamine by hydrolysis of chitosan with commercial α-amylase and glucoamylase. *J. Zhejiang Univ., Sci., B* **2011**, *12*, 931−934.
(41) Socrates, G.*Infrared and Raman Characteristic Group Frequencies: Tables and Charts*; John Wiley & Sons, 2004.
(42) Jin, X.; Wang, J.; Bai, J. Synthesis and antimicrobial activity of the Schiff base from chitosan and citral. *Carbohydr. Res.* **2009**, *344*, 825−829.
(43) Wang, S.; Zhou, S.; Huang, J.; Zhao, G.; Liu, Y. Attaching ZrO2 nanoparticles onto the surface of graphene oxide via electrostatic self-assembly for enhanced mechanical and tribological performance of phenolic resin composites. *J. Mater. Sci.* **2019**, *54*, 8247−8261.
(44) Ayanwale, A. P.; Ruíz-Baltazar, A. d. J.; Espinoza-Cristóbal, L.; Reyes-López, S. Y. Bactericidal activity study of ZrO2-Ag2O nanoparticles. *Dose-Response* **2020**, *18*, No. 1559325820941374.
(45) Das, I.; De, G. Zirconia based superhydrophobic coatings on cotton fabrics exhibiting excellent durability for versatile use. *Sci. Rep.* **2015**, *5*, No. 18503.
(46) Aghazadeh, M.; Asadi, M.; Maragheh, M. G.; Ganjali, M. R.; Norouzi, P.; Faridbod, F. Facile preparation of MnO2 nanorods and evaluation of their supercapacitive characteristics. *Appl. Surf. Sci.* **2016**, *364*, 726−731.

https://doi.org/10.1021/acsanm.2c04105
ACS Appl. Nano Mater. XXXX, XXX, XXX−XXX

(47) Balakrishnan, G.; Velavan, R.; Batoo, K. M.; Raslan, E. H. Microstructure, optical and photocatalytic properties of MgO nanoparticles. *Results Phys.* **2020**, *16*, No. 103013.
(48) Allen, J. B.; Larry, R. F.*Electrochemical Methods Fundamentals and Applications*; John Wiley & Sons, 2001.
(49) Khan, I.; Pandit, U. J.; Wankar, S.; Das, R.; Limaye, S. N. Fabrication of electrochemical nanosensor based on polyaniline film-coated AgNP-MWCNT-modified GCE and its application for trace analysis of fenitrothion. *Ionics* **2017**, *23*, 1293−1308.
(50) Jangid, K.; Gupta, R.; Sahu, R. P.; Zhitomirsky, I.; Puri, I. K. Influence of conductive porous electrodes on the apparent electrode kinetics of fenitrothion. *J. Electroanal. Chem.* **2022**, *910*, No. 116200.
(51) Janković, I. A.; Saponjic, Z. V.; Comor, M. I.; Nedeljkovic, J. M. Surface modification of colloidal TiO2 nanoparticles with bidentate benzene derivatives. *J. Phys. Chem. C* **2009**, *113*, 12645−12652.
(52) Ata, M. S.; Liu, Y.; Zhitomirsky, I. A review of new methods of surface chemical modification, dispersion and electrophoretic deposition of metal oxide particles. *RSC Adv.* **2014**, *4*, 22716−22732.
(53) Alves, M. d. F.; de Souza Corrêa, R. A. M.; da Cruz, F. S.; Franco, D. L.; Ferreira, L. F. Electrochemical enzymatic fenitrothion sensor based on a tyrosinase/poly (2-hydroxybenzamide)-modified graphite electrode. *Anal. Biochem.* **2018**, *553*, 15−23.
(54) Zhao, L.; Zhao, F.; Zeng, B. Synthesis of water-compatible surface-imprinted polymer via click chemistry and RAFT precipitation polymerization for highly selective and sensitive electrochemical assay of fenitrothion. *Biosens. Bioelectron.* **2014**, *62*, 19−24.
(55) Salehzadeh, H.; Ebrahimi, M.; Nematollahi, D.; Salarian, A. A. Electrochemical study of fenitrothion and bifenox and their simultaneous determination using multiwalled carbon nanotube modified glassy carbon electrode. *J. Electroanal. Chem.* **2016**, *767*, 188−194.
(56) Anandhakumar, S.; Mathiyarasu, J. Detection of lead (II) using an glassy carbon electrode modified with Nafion, carbon nanotubes and benzo-18-crown-6. *Microchim. Acta* **2013**, *180*, 1065−1071.
(57) Xu, H.; Peng, J.; Zhu, M.; Liu, J. Ultrasensitive detection of nitrite based on gold-nanoparticles/polyrhodamine B/carbon nanotubes modified glassy carbon electrode with enhanced electrochemical performance. *Int. J. Electrochem. Sci.* **2017**, *12*, 10642−10659.

https://doi.org/10.1021/acsanm.2c04105
ACS Appl. Nano Mater. XXXX, XXX, XXX−XXX